Hindawi
Journal of Nanomaterials
Volume 2020, Article ID 8349480, 13 pages
https://doi.org/10.1155/2020/8349480

Research Article

Enhanced Photocatalytic Activity of TiO_2/SnO_2 Binary Nanocomposites

Tetiana A. Dontsova, Anastasiya S. Kutuzova, Kateryna O. Bila, Svitlana O. Kyrii, Iryna V. Kosogina, and Daria O. Nechyporuk

Department of Inorganic Substances, Water Purification and General Chemical Technology, Chemical Technology Faculty, National Technical University of Ukraine "Igor Sikorsky Kyiv Polytechnic Institute", 03056, Prosp. Peremohy 37, Kyiv, Ukraine

Correspondence should be addressed to Tetiana A. Dontsova; dontsova@xtf.kpi.ua

Received 22 May 2020; Revised 31 July 2020; Accepted 1 August 2020; Published 18 August 2020

Academic Editor: Yasuhiko Hayashi

The paper presents the results of characterization and study of adsorption-photocatalytic properties of commercial and synthesized-by-hydrothermal method TiO_2 and TiO_2-SnO_2 nanocomposites. Hydrothermal synthesis of TiO_2-based nanocomposites was performed in two ways: single-stage and two-stage methods. Characterization was carried out by XRD, X-ray fluorescence method, XPS, EPR, PL, and low-temperature adsorption-desorption of nitrogen, which showed that TiO_2-SnO_2 nanostructured composites were obtained with tin(IV) oxide content of 10 wt.% and had acidic surface and different porous structures. Besides, modification of a commercial sample with tin(IV) oxide led to a slight decrease in the specific surface area, while modification of a synthesized-by-hydrothermal method TiO_2 sample led to an increase. It was found that sorption properties of the obtained nanocomposites and pure TiO_2 are better towards anionic dyes. Photocatalytic activity, on the contrary, is higher towards cationic dyes, which is consistent with additional studies on the destruction of these dyes. It was established that in terms of photocatalytic activity, TiO_2-SnO_2 nanocomposites are more promising than solid solutions, and modification of TiO_2 with tin(IV) oxide, in general, leads to improvement of its photocatalytic activity.

1. Introduction

Advanced Oxidation Processes (AOPs) used to remove organic pollutants from wastewater can be fairly considered to be green technologies for environmental restoration, which attributes them to safe and sustainable water treatment technologies [1, 2]. These technologies include: ozonation, ultrasound, microwaves, γ-irradiation, Fenton-like processes, homogeneous and heterogeneous photocatalysis. Among these processes, heterogeneous photocatalysis seems, in our opinion, to be the most promising due to advantages such as mild conditions and short process duration and no use of chemical reagents. Besides, photocatalysts remain chemically unchanged during and after the photocatalytic process and can be reused several times. A promising photocatalyst for the oxidation of organic compounds in aqueous media is nanodispersed titanium(IV) oxide (TiO_2) due to its high surface area, biological and chemical stability, low cost, low toxicity, and high photocatalytic activity [3–5].

Titanium(IV) oxide has been one of the most studied nanomaterials in recent decades due to its high potential for use in the energy sector and for environmental protection. Also, there are many other areas of TiO_2 application: disinfectants and antibacterial agents, self-cleaning surfaces, food and pharmaceutical additives, pigments, etc. [6–8].

TiO_2 exists in nature in three modifications: rutile (tetragonal crystal lattice), anatase (tetragonal crystal lattice), and brookite (rhombic crystal lattice). In all cases, crystal structures consist of TiO_6 octahedra [9, 10]. Figure 1 shows crystal lattices and structures of TiO_2 modifications.

It is known [12] that TiO_2 in the anatase form shows higher photocatalytic activity compared to rutile and brookite. This is explained as follows: the band gap for anatase is approximately 3.2 eV, while for rutile ~3.0 eV, indicating

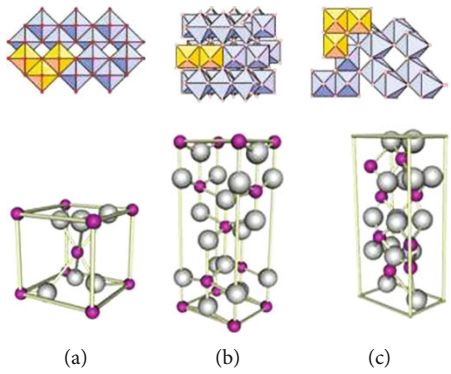

Figure 1: Crystal lattices and structures of TiO_2 modifications: (a) rutile, (b) anatase, and (c) brookite [10, 11].

better light absorption by rutile than anatase. But, according to the data on photoconductivity [13], the lifetime of the electron-hole pair is longer in anatase than in rutile, and therefore, there are more charge carriers in anatase.

Despite all the abovementioned advantages of TiO_2 as a photocatalyst, its commercial application is still limited because of its low photoactivity under visible light and fast recombination of photoexcited electrons and holes leading to poor efficiency. To enhance efficiency and usage of titanium(IV) oxide in a wide range of technological conditions, namely, under solar radiation, TiO_2 is doped and modified and nanocomposites are created on its basis [14, 15]. It should also be noted that improvement of TiO_2 photocatalytic activity can be also achieved by varying its morphology, combining different crystal modifications of TiO_2, and increasing its specific surface area [9, 16].

To increase TiO_2 efficiency under visible light, metal doping is widely used. Photoactivity of metal-doped TiO_2 photocatalysts largely depends on the nature of the doping ion, its level in the structure of titanium(IV) oxide, doping method, modification of TiO_2 being doped, etc. TiO_2 doping with metals is considered to result in overlapping of titanium 3d orbitals with d-levels of metals, which makes such TiO_2 photoactive in the visible region [14]. It was found [17] that doping of TiO_2 nanoparticles with Li, Na, Mg, Fe, and Co ions expands the range of photocatalytic reaction to visible light. In the sample doped with sodium, titanium exists as Ti^{4+} and Ti^{3+}. Conversion established between them prevented recombination of electrons (e^-) and holes (h^+).

It has been shown that doping with metal ions promotes formation of crystalline TiO_2 phases that can generate electrons (e^-) and holes (h^+) to a greater extent. Doping TiO_2 with nonmetals such as C, B, I, F, S, and N leads to its even greater photocatalytic activity in the visible region compared to metal doping [18]. This effect is associated with impurity states near the edge of the valence band, and as they do not act as charge carriers, their role as recombination centers is minimized. It was found that TiO_2 nanoparticles, doped with nitrogen and carbon, show higher photocatalytic activity when irradiated with visible light compared to TiO_2 doped with other nonmetallic dopants. The modification method is also widely studied to increase photoactivity of pure TiO_2. As TiO_2 modifiers, most attention is paid to nanoparticles of noble metals, such as Ag, Pt, Pd, Rh, and Au [19]. In this case, nanoparticles of the noble metal act as a transfer in the transport of photogenerated electrons in TiO_2 particles. Photocatalytic activity increases in this case because the recombination rate of charge carriers decreases.

Undoubtedly, creation of nanocomposites is a promising method to increase photocatalytic activity of photocatalysts [20–22]. TiO_2-based nanocomposites are created to increase efficiency of photon utilization in them under ultraviolet and visible radiation. Metal oxides such as SnO_2, ZnO, WO_3, and Fe_2O_3 are used for this purpose. Among these metal oxides, SnO_2 plays an essential role in nanocomposite structures with TiO_2 due to the production of more hydroxyl radicals in such a composite compared to others [23]. Titanium(IV) oxide and tin(IV) oxide have similar ionic radii of the cations (0.605 Å for Ti^{4+} and 0.69 Å for Sn^{4+}) and have similar structural (tetragonal structure of rutile type) and electronic properties [24]. Band gaps of SnO_2 and TiO_2 (anatase) and TiO_2 (rutile) are 3.6 eV and 3.2 eV and 3.0 eV, respectively, while the conduction band of tin(IV) oxide is approximately 0.5 V more positive than one of the titanium(IV) oxide conduction bands [11]. Therefore, creation of such composites is very promising due to possibility of efficient charge separation between crystalline phases of oxides that increases the lifetime of charge carriers and, therefore, reduces the probability of their recombination. As a result, electrons are localized in the conduction band of tin(IV) oxide, while holes are located in the valence band of titanium(IV) oxide. Thus, simultaneous combination of two different semiconductors and two phases with different energy levels can significantly increase mobility of the charge carriers, preventing their recombination and thus improving photoactivity of such a composite photocatalyst [23, 25].

Currently, there are many studies on the creation of TiO_2-SnO_2 nanocomposites to increase photoactivity. In papers [26–28], TiO_2-SnO_2 nanocomposites were synthesized, which indicate that, depending on their synthesis method and precursor type, powders with a wide range of properties could be obtained. At the same time, it is possible to obtain both metal oxides TiO_2-SnO_2 and solid solutions $Ti_xSn_{1-x}O_2$. In particular, the authors of article [26] obtained both nanocomposites TiO_2-SnO_2 and their solid solutions by sol-gel method. The latter is quite possible due to the structural analogy of TiO_2 with SnO_2, and in study [26], it occurs when molar content of Sn in composites is less than 15 wt.%. Other researchers [27] also synthesized TiO_2-SnO_2 nanoparticles by sol-gel method from titanium(IV) n-butoxide and tin(II) ethylhexanoate precursors. They found that at low concentrations of the tin precursor, TiO_2 particles formed solid solutions when being doped, while TiO_2-SnO_2 nanocomposites were obtained at high concentrations of the tin precursor. This fact confirms the results of the previously considered study. In paper [28], synthesis of TiO_2-SnO_2 nanoparticles was carried out by hydrolysis under hydrothermal conditions from anhydrous titanium and tin chlorides. Formation of solid solutions in the whole molar ratio was shown. Such different results also indicate a significant influence of the precursor type used to create TiO_2-SnO_2 systems. Even in the synthesis of pure TiO_2 from different precursors,

it is possible to obtain both monophase powders and nanocomposite particles consisting of different TiO_2 phases [29]. All this indicates that, despite the considerable amount of work devoted to the synthesis of TiO_2-SnO_2 nanocomposites, there are still more questions than answers about the physicochemical characteristics of the resulting binary systems and the impact on these characteristics of precursor types, methods, used ratios, etc. In addition, an increase in TiO_2 photocatalytic activity is observed both in the case of TiO_2-SnO_2 nanocomposite synthesis and in obtaining solid solutions. However, according to the literature data, higher photocatalytic activity is associated with TiO_2-SnO_2 nanocomposite structures, rather than their solid solutions [27].

For obtaining TiO_2-SnO_2 nanocomposites in the form of both powders and films, various methods are used, such as sol-gel [30–33], hydrothermal synthesis [34–36], chemical vapor deposition [37], spray and laser pyrolysis [38–41], coprecipitation [42, 43], and green [44]. Each of these methods has its advantages and practical application when a certain nanocomposite structure is needed. For obtaining powdered TiO_2-SnO_2 nanocomposites, the hydrothermal synthesis method seems to be the most promising due to relative simplicity, crystallization at lower temperatures than, for example, in the case of sol-gel method or precipitation method, possibility of obtaining homogeneous nanocomposite particles of different structures, etc.

In our previous study [24], TiO_2-SnO_2 systems were synthesized and characterized, obtained by both the hydrolytic and hydrothermal methods at low tin content in composites (up to 15 wt.%) using the tin(IV) chloride precursor. In that paper, it was shown that in case of using precursors such as titanium(IV) isopropoxide and tin(IV) chloride (content in the composite 10 wt.%) in both synthesis methods, mainly solid solutions are formed, which indicates easy incorporation of Sn^{4+} ions into the crystal lattice of titanium(IV) oxide of rutile phase. For further research, hydrothermal synthesis has been chosen as a more promising synthesis method, because the powders obtained by this method were characterized by larger surface areas and developed mesoporosity and better photocatalytic properties towards dyes of different nature compared to the hydrolytic method. The literature data show greater prospects of composite nanostructures with low tin content as photocatalysts. Therefore, it is of considerable interest to obtain TiO_2-SnO_2 nanocomposite structures with a small content of tin in them.

According to [45, 46], obtaining nanocomposites with low tin concentrations is possible when using the tin(II) chloride precursor. Therefore, in this work, in contrast to [24], synthesis of TiO_2-SnO_2 nanocomposites was performed using the tin(II) chloride precursor by hydrothermal method. Besides, TiO_2-SnO_2 nanocomposites in this research were obtained by single-stage and two-stage methods. For comparison, the TiO_2-SnO_2 nanocomposite based on a commercial TiO_2 sample also was synthesized. Synthesis was performed in such a way that it was possible to compare photocatalytic properties of the obtained nanocomposites with previously obtained and studied solid solutions in paper [24]. Thus, the aim of this work was to carry out synthesis of TiO_2-SnO_2 nanocomposites and their characterization, comparison of sorption-photocatalytic properties of the obtained nanocomposites with pure TiO_2 and with similarly obtained solid solutions in article [24], and study of dye degradation of different nature by synthesized nanocomposite photocatalysts.

2. Materials and Methods

2.1. Materials. Reagents of analytical grade were used in the research: titanium(IV) isopropoxide 98+% ($C_{12}H_{28}O_4Ti$, Acros Organics, China); tin(II) chloride ($SnCl_2 \times 2H_2O$, Merck KGaA, Germany); isopropyl alcohol (C_3H_7OH, Ukraine); nitric acid (HNO_3, 65%, Merck KGaA, Germany); methylene blue dye ($C_{16}H_{18}ClN_3S$, Carlo Erba Reagents, France); Congo red dye ($C_{32}H_{22}N_6Na_2O_6S_2$, Carlo Erba Reagents, France); and titanium(IV) oxide (TiO_2, Aeroxide® TiO_2P25, Evonik, Germany).

2.2. Nanocomposite Synthesis. Nanocomposites were synthesized by hydrothermal method in two ways: single-stage and two-stage methods.

Single-stage synthesis of titanium(IV) oxide and tin(IV) oxide nanocomposites was performed as follows: 7.5 mL of isopropyl alcohol and 2.5 mL of distilled water were mixed in a Teflon reactor. To the resulting mixture, 4x prediluted nitric acid was added dropwise to pH 1.5; then, 5 mL of a titanium(IV) isopropoxide solution was slowly added under constant stirring. After that, 0.2 g of tin(II) chloride was added and stirred vigorously for 20 minutes, and then pH was measured, which was 2.6. Next, the Teflon reactor was placed in a steel autoclave and hydrothermal treatment was performed at 453 K for 12 hours. Then, the resulting suspension was cooled, centrifuged (5000 rpm, MPW-310 centrifuge, Poland), and washed until pH 6. The washed powders were dried for 12 hours at 353 K and then grounded.

Two-stage synthesis of TiO_2-SnO_2 nanocomposites was carried out as follows: first, titanium(IV) oxide was synthesized by hydrothermal method from titanium(IV) isopropoxide; then, in the presence of titanium(IV) oxide, tin(IV) oxide was synthesized. In the first stage, synthesis was carried out in the same way as in the single-stage method except from introduction of the tin(II) chloride precursor into the reaction medium [24]. Obtained in this way, pure TiO_2 was dried for 12 hours at a temperature of 353 K and grounded. Next, the second stage of nanocomposite synthesis was performed. 7.5 mL of isopropyl alcohol and 2.5 mL of distilled water were mixed in a Teflon reactor, and 1.32 g of the synthesized composites in the first stage TiO_2 (or a commercial sample) was added under stirring. After formation of a homogeneous suspension, 0.2 g of $SnCl_2$ was added under vigorous stirring. The solution thus obtained had pH of 2.5. The Teflon reactor was placed in a steel autoclave, and hydrothermal treatment was performed at 453 K for 12 hours. Then, the suspension was cooled, centrifuged (5000 rpm, MPW-310 centrifuge, Poland), and washed until pH 6. The washed powders were dried for 12 hours at 353 K and grounded.

Thus, three composites were synthesized and labeled as follows: P90TiO_2-SnO_2, s1TiO_2-SnO_2, and s2TiO_2-SnO_2

Table 1: TiO_2 samples and TiO_2-based composites.

$P25TiO_2$	Commercial sample AEROXIDE® TiO_2P25
$sTiO_2$	TiO_2 synthesized according to the method described in [21]
$1P25TiO_2$-SnO_2	Commercial AEROXIDE® TiO_2P25 modified with tin oxide
$s1TiO_2$-SnO_2	TiO_2-SnO_2 composite synthesized by single-stage hydrothermal synthesis
$s2TiO_2$-SnO_2	TiO_2-SnO_2 composite synthesized by two-stage hydrothermal synthesis

(description is given in Table 1). Additionally, description of two other TiO_2 samples (commercial and laboratory-synthesized) is given, which were studied in this work for comparison.

2.3. Characterization of TiO_2 Samples and TiO_2-SnO_2 Composites. Chemical composition of the synthesized nanocomposites was determined by X-ray fluorescence analysis using an EXPERT 3L INAM analyzer (Ukraine). The measurement range of mass fractions (concentrations) of elements was from 0.005% to 100%.

A study of the phase composition of the samples was performed on an X-ray diffractometer Rigaku Ultima IV (Japan) with CuKα radiation (40 kW, 30 mA), calculation of which was performed automatically using standard cards: No. 00-021-1276 (rutile), No. 00-021-1272 (anatase), and No. 00-041-1445 (cassiterite). The average crystallite size was calculated by Scherrer's formula.

Nitrogen adsorption-desorption isotherms were obtained on a Quantachrome® Nova 4200e analyzer (USA). The mass of adsorbed and desorbed nitrogen was determined by a built-in algorithm based on the Langmuir or Brunauer-Emmett-Teller (BET) isotherm equation. Porous structure of the samples was determined by the Barrett-Joyner-Halenda (BJH) method.

X-ray photoelectron spectroscopy (XPS) spectra were obtained using a Kratos AXIS 165 spectrometer with Al mono Kalfa X-ray. EPR spectra were recorded at room temperature (298 K) on a RADIOPAN SE/X 2547 spectrometer. A fluorescence spectrophotometer (PerkinElmer, LS55) was used to record photoluminescence (PL) spectra. The electrons of the test samples were excited at the wavelength of 230 nm (5395 eV). For surface acidity determination, 1% suspensions of the samples were prepared, and pH of the obtained suspensions was measured for 2 hours using a Portlab 102 pH meter (Russia) according to the method described in [47].

2.4. Sorption and Photocatalytic Properties. Sorption and photocatalytic properties were evaluated by the discoloration degree of dyes of different nature (methylene blue and Congo red), as well as by the degree of their destruction.

Sorption properties of the samples were studied as follows: 0.05 g of a photocatalyst sample was added to 50 mL of a dye solution (methylene blue (MB), $C_{16}H_{18}ClN_3S$ or Congo red (CR), $C_{32}H_{22}N_6Na_2O_6S_2$) and stirred in an ultrasonic bath (40 kHz, UZM-004-1, Ukraine). Then, the resulting suspension was stirred for another 20 minutes on a magnetic stirrer, and the spent catalyst was separated from the solution by centrifugation. Concentration of the dye in the solutions before and after sorption was determined using spectrophotometer UV-5800PC (Shanghai Metash Instruments, China).

A study of the photocatalytic properties of the samples was performed similarly, except that UV irradiation of the suspension (368 nm) was additionally used during stirring on a magnetic stirrer for 20 minutes.

The discoloration degree (%) of a dye solution was determined by relative change in optical density of the dye solutions (for methylene blue dye, it was measured at a wavelength of 664 nm; for Congo red dye, the wavelength was 505 nm):

$$X = \frac{A_0 - A_1}{A_0} \times 100, \quad (1)$$

where A_0 is the optical density of the initial dye solution and A_1 is the optical density of the solution after experiment.

Destruction of dyes was studied by absorption of CO_2 released in the photocatalytic process by alkali, followed by its recalculation into organic carbon content. The process of dye destruction was carried out on an experimental installation of original design, the main elements of which were a quartz flask and a gas absorption flask, tightly connected. Dye solution and catalyst were placed in a quartz flask and stirred using sonication for 5 minutes. Next, the quartz flask was connected to the gas absorption flask, into which 25 mL of sodium hydroxide solution (concentration 0.1 mol•L^{-1}) had been poured, and then vacuum was created in it. After this, photocatalytic destruction was performed by stirring under ultraviolet radiation (368 nm). CO_2 gas released as a result of the photocatalytic process bubbled into the gas absorption flask and was absorbed by alkali solution, the change in concentration of which was determined by titration with hydrochloric acid (concentration 0.1 mol•L^{-1}).

3. Results and Discussion

The following transformations took place in the process of nanocomposite synthesis:

$$Ti(OCH(CH_3)_2)_4 + 2H_2O = TiO_2 + 4(CH_3)_2CHO \quad (2)$$

$$2SnCl_2 + O_2 + H_2O = 2SnO_2 + 4HCl \quad (3)$$

Synthesis of titanium(IV) oxide was carried out according to reaction (2), and formation of tin(IV) oxide by both single-stage and two-stage hydrothermal syntheses occurred according to reaction (3).

3.1. XRD. Figure 2 shows X-ray patterns of all obtained samples that were automatically analyzed. Standard cards were used for identification: anatase, JCPDS 01-070-7348; rutile, JCPDS 01-070-7347; and cassiterite, JCPDS 00-041-1445.

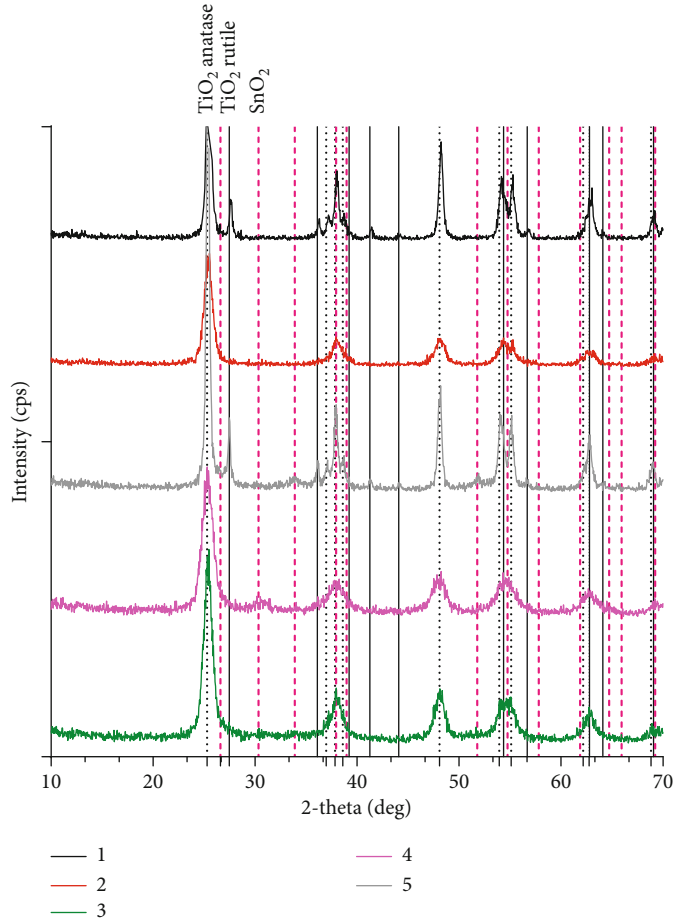

Figure 2: Diffraction patterns of the samples: 1: TiO_2P25; 2: sTiO_2; 3: P25TiO_2-SnO_2; 4: s1TiO_2-SnO_2; and 5: s2TiO_2-SnO_2.

Table 2: XRD analysis.

Sample	Phase	a (nm)	b (nm)	c (nm)	Crystallite size (nm)	Mass content (%)
P25TiO_2	Anatase	0.378	0.378	0.950	4.4	75
	Rutile	0.459	0.459	0.296	4.0	25
sTiO_2	Anatase	0.378	0.378	0.947	7.0	100
P25TiO_2-SnO_2	Anatase	0.379	0.379	0.950	15.2	69
	Rutile	0.459	0.459	0.296	20.1	21
	SnO_2	0.475	0.475	0.319	11.6	10
s1TiO_2-SnO_2	Anatase	0.379	0.379	0.945	5.7	89
	SnO_2	0.497	0.497	0.497	5.2	11
s2TiO_2-SnO_2	Anatase	0.379	0.379	0.949	7.0	89
	SnO_2	0.483	0.483	0.321	6.8	11

As a result of the analysis, it has been established (Table 2) that a commercial sample of TiO_2P25 consists of approximately 25% rutile and 75% anatase that corresponds to the literature data [44], while hydrothermally synthesized sample sTiO_2 has pure anatase modification. Phase composition analysis of nanocomposites P25TiO_2-SnO_2, s1TiO_2-SnO_2, and s2TiO_2-SnO_2 (Table 2) shows that nanocomposites have similar phase composition of pure TiO_2 and additional phase of cassiterite, the content of which is 10-11% that corresponds to the theoretical calculation.

Analysis of structural characteristics of nanocomposites and TiO_2 samples (Table 2) shows that parameters a, b, and c of crystal lattices for all phases are quite close to the theoretical values ($a = 0.379$ nm and $c = 0.951$ nm for anatase; $a = 0.459$ nm and $c = 0.296$ nm for rutile; and $a = 0.474$ nm and $c = 0.318$ nm for cassiterite). Therefore, significant distortions of crystal lattices are not observed.

Crystallite sizes of all samples are in the range of 4.0-20.1 nm. Thus, all samples are nanocrystalline. P25TiO_2-SnO_2 nanocomposite, based on the commercial sample AEROXIDE® TiO_2P25, has the largest crystallite size that is probably because of the aggregation of initial particles. Nanocomposites based on synthesized TiO_2 have smaller crystallite sizes, and for s1TiO_2-SnO_2 nanocomposite obtained by single-stage synthesis, crystallite sizes are smaller than those for pure TiO_2 and s2TiO_2-SnO_2 nanocomposites synthesized in two stages. Thus, single-stage synthesis allows obtaining TiO_2-SnO_2 nanocomposites with smaller crystallite size. The two-stage method in case of using the commercial TiO_2 sample promotes its aggregation but does not change the crystallite size of the hydrothermally synthesized pure TiO_2.

3.2. Chemical Composition. Chemical analysis of the samples confirmed 10 wt.% content of cassiterite. The results of chemical analysis are presented in Table 3. Thus, based on XRD results and taking into account chemical composition of TiO_2-SnO_2 nanocomposites, it can be stated that in all cases, nanocomposites were obtained with cassiterite phase content of 10 wt.%.

3.3. XPS, EPR, and PL. Chemical composition and available surface chemical states of TiO_2-SnO_2 nanocomposites were studied by XPS method. Obtained survey spectra for nanocomposites and synthesized TiO_2 are shown in Figure 3 and indicate the presence of Ti, Sn, O, and C (hydrocarbons from the XPS device). An XPS data report showed the presence of the following surface states: Ti^{3+} and Ti^{4+} for titanium and Sn^{4+} for tin. Besides, tin concentration in the P25TiO_2-SnO_2 and s2TiO_2-SnO_2 composites is higher (6.1-6.5%) than that in the s1TiO_2-SnO_2 (3.9%) sample. That is due to the fact that P25TiO_2-SnO_2 and s2TiO_2-SnO_2 nanocomposites were obtained by two-stage synthesis, and in this case, tin was deposited on the surface. s1TiO_2-SnO_2 nanocomposite was synthesized via single-stage synthesis, so tin was distributed in the whole material volume.

In addition, Supplementary Materials contains native XPS spectra of Ti 2p, Sn 3d, and O 1s for TiO_2-SnO_2 nanocomposites (Figures S1 , S2, and S3, respectively). According to the spectra of Ti 2p (Figure S1), 2 peaks are observed: the first is about 464 eV, which corresponds to the binding energy of Ti 2p 1/2, and the second is about 459 eV, which refers to the binding energy of Ti 2p 3/2 [21]. In the XPS spectra of Sn 3d for all nanocomposites (Figure S2), two peaks were also present that correspond to the binding energy at approximately 495 eV and 486 eV and are characteristic for Sn 3d 3/2 and Sn 3d 5/2, respectively [48–50]. XPS spectra of O 1s (Figure S3) for P25TiO_2-SnO_2 and s2TiO_2-SnO_2 composites are characterized by peaks at 530 eV, 530.5 eV, and 535.5 eV that correspond to oxygen bound in TiO_2 and SnO_2 and in the form of surface hydroxyl oxygen (OH), respectively [51–53]. s1TiO_2-SnO_2 nanocomposite is characterized by similar peaks except the one corresponding to hydroxyl oxygen.

Also, EPR spectra (Figure S4) of TiO_2P25, sTiO_2, P25TiO_2-SnO_2, s1TiO_2-SnO_2, and s2TiO_2-SnO_2 are shown in Supplementary Materials. The EPR spectra obtained at room temperature demonstrate weak signals, which is most likely associated with the short lifetime of electrons and holes under these conditions.

Table 3: Chemical composition of TiO_2-SnO_2 composites.

	P25TiO_2-SnO_2	s1TiO_2-SnO_2	s2TiO_2-SnO_2
Element	Mass fraction (%)		
22Ti	90.5	88.1	89.5
50Sn	9.5	11.9	10.5

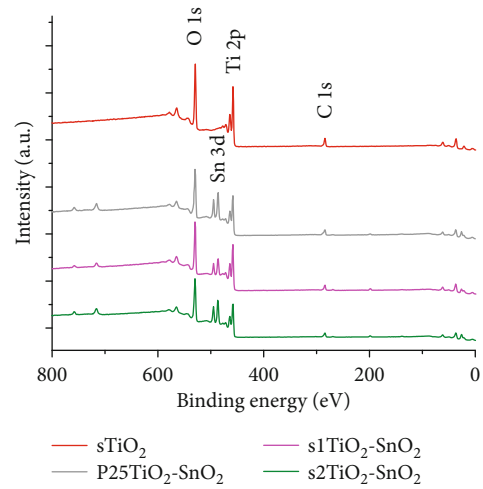

Figure 3: XPS spectra of TiO_2-SnO_2 nanocomposites and TiO_2 synthesized by hydrothermal method.

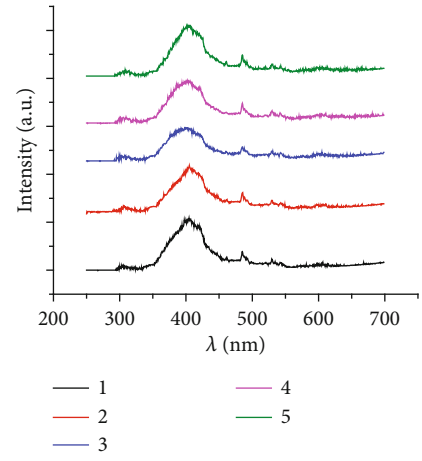

Figure 4: PL spectra: 1: TiO_2P25; 2: sTiO_2; 3: P25TiO_2-SnO_2; 4: s1TiO_2-SnO_2; and 5: s2TiO_2-SnO_2.

Figure 4 shows photoluminescence spectra of the samples. As can be seen from Figure 4, all samples demonstrate an emission at the wavelength of 405-406 nm (~3.08 eV), the intensity of which is approximately the same. However, peak intensity is the highest for the samples TiO_2P25 and s2TiO_2-SnO_2 and the lowest for the P25TiO_2-SnO_2 sample. This indicates that among all samples, the TiO_2P25 and s2TiO_2-SnO_2 samples have the highest charge recombination rate, while the P25TiO_2-SnO_2 sample has the lowest [54].

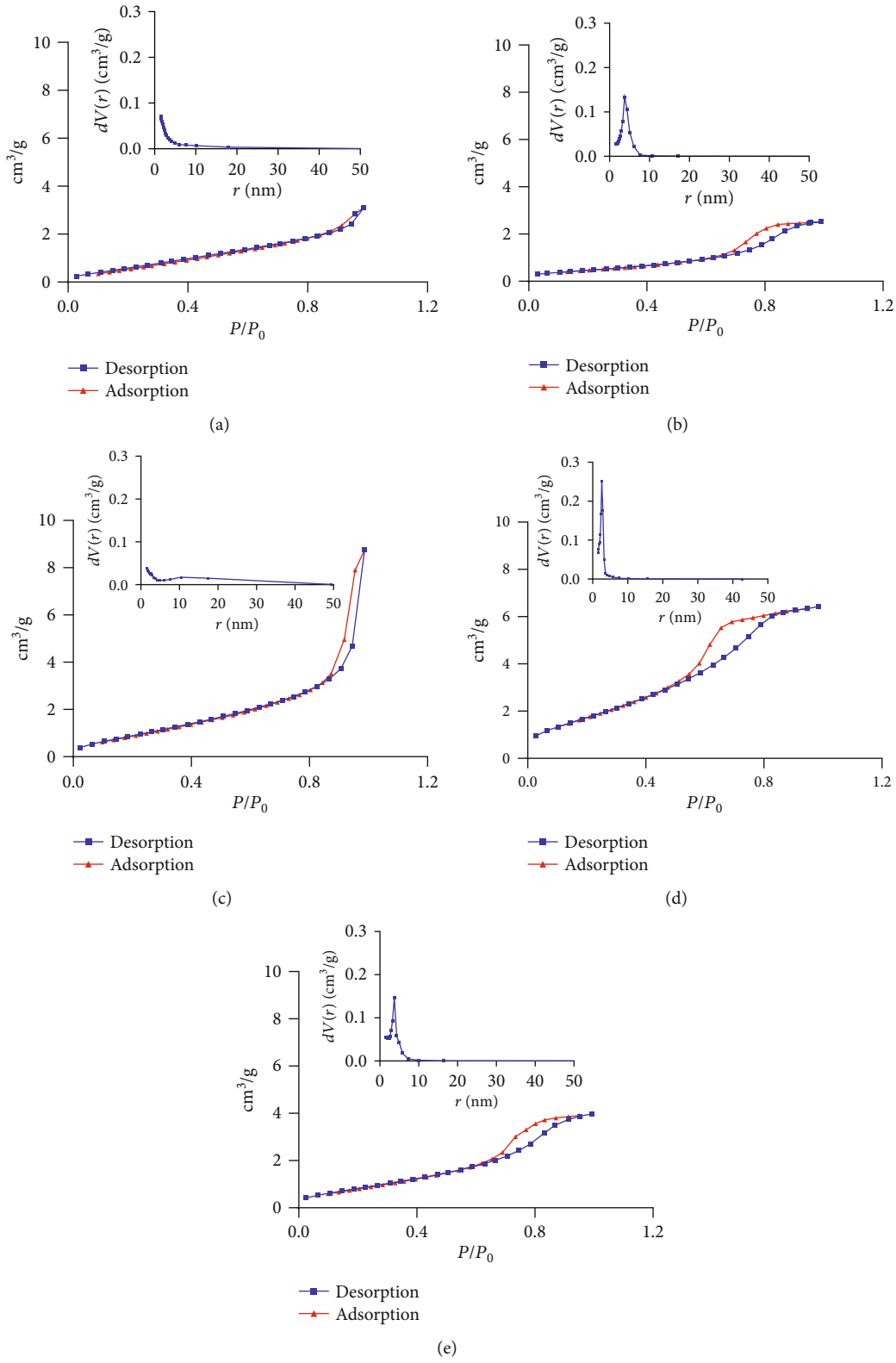

Figure 5: Nitrogen adsorption-desorption isotherms and pore size distribution: (a) TiO_2P25, (b) sTiO_2, (c) P25TiO_2-SnO_2, (d) s1TiO_2-SnO_2, and (e) s2TiO_2-SnO_2.

3.4. Structural-Adsorption Characteristics. Figure 5 presents the isotherms of nitrogen adsorption-desorption and pore size distribution for all tested samples. As can be seen from the presented isotherms, all samples have different porous structures. Thus, according to the IUPAC classification, the P25TiO_2 sample has isotherm type III, which is typical of

Table 4: Structural-adsorption characteristics of nanocomposites.

Sample	Specific surface area (m^2/g)	Average pore diameter (nm)	Total pore volume (cm^3/g)
$P25TiO_2$	109	—	—
$sTiO_2$	172	3.8	0.32
$P25TiO_2$-SnO_2	99	1.5	0.25
$s1TiO_2$-SnO_2	223	2.6	0.28
$s2TiO_2$-SnO_2	192	3.7	0.31

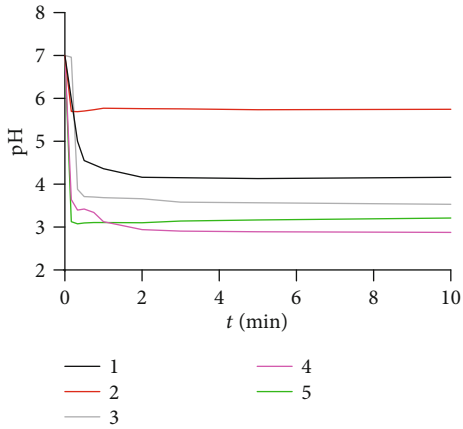

Figure 6: Total acidity of sample surface: 1: TiO_2P25; 2: $sTiO_2$; 3: $P25TiO_2$-SnO_2; 4: $s1TiO_2$-SnO_2; and 5: $s2TiO_2$-SnO_2.

nonporous or macroporous materials. The isotherm of the commercial sample $P25TiO_2$ after modification with tin(IV) oxide has a slightly different form; namely, isotherm type III has transformed into type V. This indicates transition of a nonporous or macroporous structure to a mesoporous-microporous structure that has developed as a result of the modification. It can also be seen that synthesized samples of $sTiO_2$, $s1TiO_2$-SnO_2, and $s2TiO_2$-SnO_2 are characterized by isotherms of type IV, which are characteristic for mesoporous materials [55].

Nature of hysteresis loops for samples $P25TiO_2$-SnO_2, $sTiO_2$, $s1TiO_2$-SnO_2, and $s2TiO_2$-SnO_2 is different. Therefore, they have different pore structures. According to the IUPAC classification, the hysteresis loop of the $P25TiO_2$-SnO_2 sample belongs to the H3 type, which is characteristic of lamellar structures with the presence of macropores [55].

Thus, as a result of modification of commercial TiO_2 surface, small mesoporosity developed. At the same time, the specific surface area decreased slightly from 109 m^2/g for $P25TiO_2$ to 99 m^2/g for $P25TiO_2$-SnO_2 (Table 4), which may indicate slight aggregation of titanium(IV) oxide particles as a result of modification. The synthesized $sTiO_2$ sample has a hysteresis loop of type H4 [55], which indicates mesoporous-microporous structure of this sample. The structure of $s2TiO_2$-SnO_2 nanocomposite is close to the structure of $sTiO_2$, which is quite understandable since it

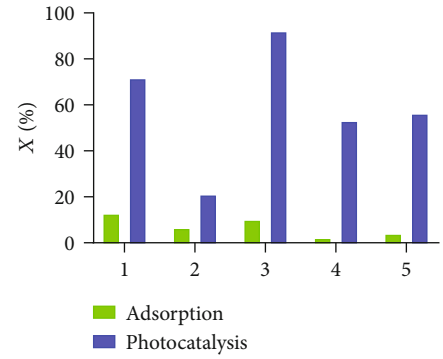

Figure 7: Adsorption and photocatalytic studies using methylene blue (dye concentration 10 mg/L, reaction time 20 min): 1: TiO_2P25; 2: $sTiO_2$; 3: $P25TiO_2$-SnO_2; 4: $s1TiO_2$-SnO_2; and 5: $s2TiO_2$-SnO_2.

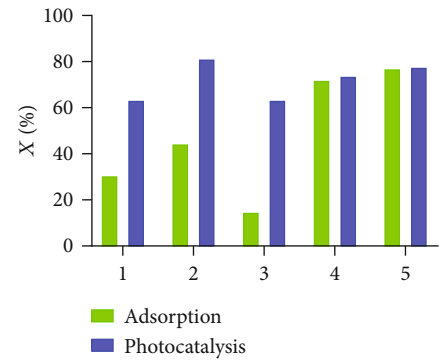

Figure 8: Adsorption and photocatalytic studies using Congo red (dye concentration 40 mg/L, reaction time 20 min): 1: TiO_2P25; 2: $sTiO_2$; 3: $P25TiO_2$-SnO_2; 4: $s1TiO_2$-SnO_2; and 5: $s2TiO_2$-SnO_2.

was obtained by modification of $sTiO_2$ with tin(IV) oxide, which led to a small change in porous structure of titanium(IV) oxide. As the result of modification, the surface area increased slightly from 172 m^2/g for $sTiO_2$ to 223 m^2/g for $s2TiO_2$-SnO_2. Different methods of obtaining pure TiO_2 explain this unequal effect on the specific surface area due to modification. Probably, hydrothermal conditions under which modification took place caused aggregation of the commercial sample particles, in contrast to the synthesized $sTiO_2$ under the same conditions. The hysteresis loop of the $s1TiO_2$-SnO_2 sample belongs to the H2 type (*b*), which is characteristic of complex porous structures that have pores with a large neck diameter [55].

Obtained structural characteristics (average pore diameter and total pore volume) for all samples correlate well with the types of isotherms and porous structures.

3.5. Surface Acidity. Figure 6 illustrates the change in pH of all test sample suspensions according to the method presented in [43]. The shape of curves indicates that all samples have Lewis acid centers, and based on the slope of the curves, the largest number of the centers belong to $s1TiO_2$-SnO_2 and $s2TiO_2$-SnO_2 nanocomposites. Of particular

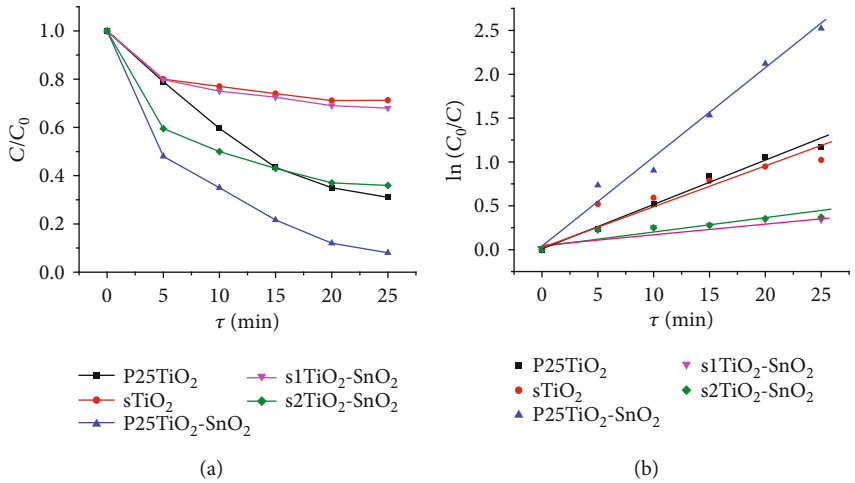

Figure 9: Change in the concentration of MB during the photocatalytic process: (a) kinetic dependences C/C_0 and (b) linearized curves ln (C_0/C).

Table 5: Apparent rate constants (K) and coefficients of determination (R^2) of linearized kinetic curves.

Sample	K (min^{-1})	R^2
P25TiO$_2$	0.0624	0.976
sTiO$_2$	0.0572	0.965
P25TiO$_2$-SnO$_2$	0.1089	0.967
s1TiO$_2$-SnO$_2$	0.0074	0.973
s2TiO$_2$-SnO$_2$	0.0079	0.951

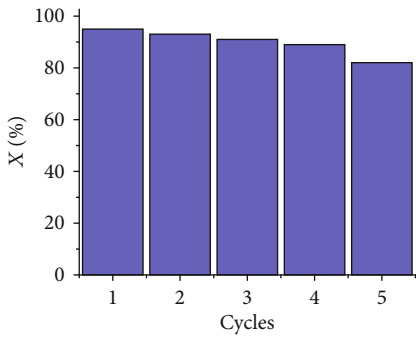

Figure 10: Degree of photocatalytic removal of MB in reusability tests with the P25TiO$_2$-SnO$_2$ sample (dye concentration 10 mg/L, reaction time 20 min).

interest is s1TiO$_2$-SnO$_2$ nanocomposite; change in pH of its suspensions was established very quickly and did not change over time. This behavior indicates the presence of mainly Lewis centers and is confirmed by its XPS spectra, in which there are no surface OH groups present.

After 2 hours (when equilibrium was achieved), the isoionic point (pH$_{iip}$) value was 4.15 for P25TiO$_2$, 5.78 for sTiO$_2$, 3.53 for P25TiO$_2$-SnO$_2$, 2.84 for s1TiO$_2$-SnO$_2$, and 3.33 for s2TiO$_2$-SnO$_2$. pH$_{iip}$ values indicate acidic nature of the surface for all samples. In this case, sTiO$_2$ is characterized by the lowest acidity, while s1TiO$_2$-SnO$_2$ nanocomposite by the highest. Comparing pH$_{iip}$ of pure TiO$_2$ samples and TiO$_2$-based composites, it can be seen that modification with SnO$_2$ in all cases increases acidity. It should be noted that despite the lower acidity of the sTiO$_2$ sample in comparison with P25TiO$_2$, modification of their surface with tin(IV) oxide leads to different results. Acidity of the nanocomposites based on sTiO$_2$ is much higher than in the case of a composite based on a commercial sample. This is probably due to the modification in acidic media and larger specific surface area of sTiO$_2$ compared to P25TiO$_2$ that resulted in greater sorption of H$^+$ ions by the sTiO$_2$ surface from the reaction solution during synthesis.

3.6. Adsorption-Photocatalytic Properties. Adsorption and photocatalytic activity of all samples was studied using the most widely used model dye solutions of different nature: methylene blue (cationic dye) and Congo red (anionic dye) [56, 57].

Results of the adsorption and photocatalytic study on methylene blue are shown in Figure 7. Diagram data show that methylene blue is almost not adsorbed on the samples. This is because of the acidity of all samples resulting in total positive charge of their surface that eventually caused low cationic dye adsorption.

Photocatalytic activity (Figure 7) is higher, and the dye removal degree in photocatalysis ranges from 50% to 90%. The best results were shown by a modified commercial sample P25TiO$_2$-SnO$_2$ that indicates a positive effect of modification. A similar situation is observed in case of modified and unmodified samples: modification leads to an increase in photocatalytic degradation of methylene blue from 21% for sTiO$_2$ to 53% for s1TiO$_2$-SnO$_2$ and 56% for s2TiO$_2$-SnO$_2$.

Figure 8 illustrates adsorption-photocatalytic properties of all test samples regarding Congo red. Adsorption properties of almost all samples are much better towards anionic dye, and adsorption efficiency ranges from 10% to 78%. Photocatalytic extraction of Congo red is slightly greater than adsorption and, in general, does not indicate significant differences for modified and unmodified samples.

Table 6: Comparative table of photocatalysis and destruction under UV radiation (368 nm).

Sample	Photocatalysis (%)		Destruction (%)	
	Methylene blue	Congo red	Methylene blue	Congo red
No sample, only UV radiation	—	—	18	5
P25TiO_2	65	61	36	10
sTiO_2	21	80	25	10
P25TiO_2-SnO_2	92	63	52	48
s1TiO_2-SnO_2	53	74	52	10
s2TiO_2-SnO_2	56	78	44	9
TiO_2-SnO_2 obtained in [24]	31	75	—	—

Supplementary Materials contains absorption spectra of initial dye solutions (S5) and solutions after photocatalytic extraction of cationic (S6) and anionic (S7) dyes. In general, they indicate a decrease in dye concentration after the photocatalytic process. However, in some cases, dye concentration did not change or even increase, or peaks of initial dye solutions were observed in the ultraviolet region, for which the degradation degree was not calculated. In addition, when Congo red was treated using the s1TiO_2-SnO_2 and s2TiO_2-SnO_2 samples, the main absorption peak of the anionic dye was shifted, caused by high acidity of these samples.

In addition, kinetic dependences were obtained regarding degradation of the most widely used dye in photocatalytic studies—methylene blue. Figure 9 shows photocatalytic removal of MB utilizing each photocatalyst sample over time. As seen from Figure 9(a), the P25TiO_2-SnO_2 sample is the most efficient to remove MB from its aqueous solution. This is consistent with the results shown in Figure 7 and is explained by the lower recombination rate according to PL spectra.

Figure 9(b) shows linearized kinetic curves, determination coefficients (R^2, Table 5) of which indicate that reaction kinetics for all samples is adequately described by the Langmuir-Hinshelwood model, being in full agreement with the literature data [58–60]. The corresponding apparent rate constants (K, Table 5) confirm the previously obtained results regarding the highest photocatalytic activity of the P25TiO_2-SnO_2 sample (apparent rate constant of which is 1.75 times higher than that of unmodified TiO_2P25).

Thus, subsequent studies on the stability and reusability of the obtained photocatalysts were carried out utilizing the P25TiO_2-SnO_2 sample.

Figure 10 shows results of the reusability tests of the P25TiO_2-SnO_2 sample in photocatalytic extraction of MB. As can be seen from the diagram, a high degree of dye removal (95-82%) by the chosen photocatalyst is observed during five cycles, which slightly decreases by the end of the fifth cycle. The obtained results indicate good stability and reusability of the tested photocatalyst.

3.7. Dye Destruction and Analysis of Photocatalytic Studies. Additionally, it was decided to study destruction of methylene blue and Congo red (by the amount of CO_2 released) in the photocatalytic process for its deeper understanding. Table 6 shows destruction results and, for comparison, photocatalytic extraction data (obtained by spectrophotometric method). The photocatalytic extraction degree of dyes by the TiO_2-SnO_2 sample obtained hydrothermally but from different precursors (tin(IV) chloride [24], which resulted in a TiO_2 solid solution formation) is also mentioned in Table 6.

As can be seen from Table 6, dye degradation under UV radiation (368 nm) occurs even without photocatalysts and is approximately 18% for methylene blue and 5% for Congo red. Destruction of methylene blue with photocatalysts is greater and is even higher in case of the photocatalytic process utilizing modified samples of TiO_2, both commercial and synthesized. In general, the destruction degree is lower than the photocatalytic extraction degree that indicates partial extraction of methylene blue either due to sorption or due to decomposition into smaller structural units. A similar pattern is observed for Congo red. At the same time, the degradation degree of Congo red is lower than that of methylene blue and much lower than its photocatalytic extraction degree. Therefore, anionic dye extraction occurs more due to adsorption interactions or due to its decomposition into smaller structural units. The lower destruction degree of Congo red compared to methylene blue can be explained by the fact that more energy is required for the complete destruction of a large Congo red molecule. It should be added that the destruction degree of methylene blue by the P25TiO_2-SnO_2 nanocomposite is much higher (4.8 times) than by the commercial P25TiO_2 sample. Therefore, the positive effect of modification with tin(IV) oxide was also observed in case of anionic dye. Thus, results of dye photocatalytic extraction are fully consistent with the results of destruction and indicate a general positive effect of modification with tin(IV) oxide leading to increased photocatalytic activity of TiO_2.

Comparison of the results of dye photocatalytic extraction obtained in this research with the photocatalytic activity of the TiO_2-SnO_2 sample obtained in [24] (Table 6) shows better prospects of TiO_2-SnO_2 nanocomposites obtained using the tin(II) chloride precursor as evidenced by their higher photocatalytic activity towards methylene blue. Comparison of the obtained results with the results reported by other researchers, for example, in [58, 59], in which 60–75% of the dyes are removed within 20 minutes of the photocatalytic process, also indicates that development of TiO_2-SnO_2 nanocomposites is highly promising.

4. Conclusions

In the paper, TiO_2-SnO_2 nanocomposites were obtained by hydrothermal synthesis using the single-stage and two-stage methods. In addition, TiO_2-SnO_2 nanocomposite based on the commercial sample AEROXIDE® TiO_2P25 was synthesized. They were characterized by XRD, X-ray fluorescence method, XPS, EPR, PL, and low-temperature nitrogen adsorption-desorption method. The effect of TiO_2 modification with tin(IV) oxide on sorption-photocatalytic properties of obtained nanocomposites was studied.

It was found that in all cases, nanostructured TiO_2-SnO_2 composites were obtained (crystallite sizes range from 4.0 nm to 20.1 nm), which contain 10 wt.% of the SnO_2 phase. A study of the surface chemical states of TiO_2-SnO_2 nanocomposites revealed the presence of OH ions on the surface of nanocomposites obtained in two stages and their absence in the nanocomposite synthesized in one stage. The absence of hydroxide ions is confirmed by the results of a total acidity study of nanocomposite surface, according to which all samples have acidic nature of their surface.

Adsorption-structural studies have shown that the commercial sample of TiO_2 is nonporous, and its modification under hydrothermal conditions leads to a slight aggregation of TiO_2 particles and development of minor mesoporosity. TiO_2 synthesis in hydrothermal conditions, as well as creation of nanocomposites based on it, leads to obtaining mesoporous powders with a pore diameter of 2.6-3.8 nm and specific surface area in the range of 172-223 m^2/g but with different pore structures.

Sorption-photocatalytic properties of TiO_2-SnO_2 nanocomposites and pure TiO_2 powders indicate higher adsorption efficiency towards anionic dye (consistent with acidity) and higher photocatalytic activity towards cationic dye. Moreover, studies on the destruction of both dyes are consistent with photocatalytic experiments, and comparison of photocatalytic properties of TiO_2-SnO_2 nanocomposites with a previously synthesized solid solution indicates greater prospects of nanocomposites. Therefore, it can be noted that in general, TiO_2 modification by tin(IV) oxide leads to a photocatalytic activity increase.

Data Availability

No data were used to support this study.

Conflicts of Interest

The authors declare that there is no conflict of interest regarding the publication of this paper.

Supplementary Materials

S1: XPS spectra (Ti 2p) of TiO_2-SnO_2 nanocomposites. S2: XPS spectra (Sn 3d) of TiO_2-SnO_2 nanocomposites S3: XPS spectra (O 1s) of TiO_2-SnO_2 nanocomposites. S4: EPR spectra of (a) TiO_2P25, (b) sTiO_2, (c) P25TiO_2-SnO_2, (d) s1TiO_2-SnO_2, (e) s2TiO_2-SnO_2. S5: Absorption spectra of initial dyes.S6: Absorption spectra after photocatalytic removal of Methylene blue.S7: Absorption spectra after photocatalytic removal of Congo red. *(Supplementary materials)*

References

[1] S. J. Mazivila, I. A. Ricardo, J. M. M. Leitão, and J. C. G. Esteves da Silva, "A review on advanced oxidation processes: from classical to new perspectives coupled to two- and multi-way calibration strategies to monitor degradation of contaminants in environmental samples," *Trends in Environmental Analytical Chemistry*, vol. 24, p. e00072, 2019.

[2] M. M. M'Arimi, C. A. Mecha, A. K. Kiprop, and R. Ramkat, "Recent trends in applications of advanced oxidation processes (AOPs) in bioenergy production: review," *Renewable and Sustainable Energy Reviews*, vol. 121, p. 109669, 2020.

[3] W. Tu, W. Guo, J. Hu et al., "State-of-the-art advancements of crystal facet-exposed photocatalysts beyond TiO_2: design and dependent performance for solar energy conversion and environment applications," *Materials Today*, vol. 33, pp. 75–86, 2020.

[4] S. Horikoshi and N. Serpone, "Can the photocatalyst TiO_2 be incorporated into a wastewater treatment method. Background and prospects," *Catalysis Today*, vol. 340, pp. 334–346, 2020.

[5] Z. Xing, J. Zhang, J. Cui et al., "Recent advances in floating TiO_2-based photocatalysts for environmental application," *Applied Catalysis B: Environmental*, vol. 225, pp. 452–467, 2018.

[6] D. Zietal, B. Czarczynska-Goslinska, D. T. Mlynarczyk et al., "Titanium dioxide nanoparticles: prospects and applications in medicine," *Nanomaterials*, vol. 10, no. 2, p. 387, 2020.

[7] J. Moma and J. Baloyi, "Modified titanium dioxide for photocatalytic applications," *Photocatalysts - Applications and Attributes*, vol. 18, 2019.

[8] W. M. M. Mahmoud, T. Rastogi, and K. Kümmerer, "Application of titanium dioxide nanoparticles as a photocatalyst for the removal of micropollutants such as pharmaceuticals from water," *Current Opinion in Green and Sustainable Chemistry*, vol. 6, pp. 1–10, 2017.

[9] T. A. Dontsova, S. V. Nahirniak, and I. M. Astrelin, "Metaloxide nanomaterials and nanocomposites of ecological purpose," *Journal of Nanomaterials*, vol. 2019, Article ID 5942194, 31 pages, 2019.

[10] A. Stepanov, A. Xiao, and X. Ren, "Implantation of titanium dioxide with transition metalions," *In Titanium Dioxide: Applications, Synthesis and Toxicity*, vol. 52, pp. 59–83, 2013.

[11] D. A. H. Hanaor and C. C. Sorrell, "Review of the anatase to rutile phase transformation," *Journal of Materials Science*, vol. 46, no. 4, pp. 855–874, 2011.

[12] G. Cacciato, M. Zimbone, F. Ruffino et al., "TiO_2 nanostructures and nanocomposites for sustainable photocatalytic water purification," *IntechOpen*, vol. 4, pp. 51–64, 2015.

[13] H. Dong, G. Zeng, L. Tang et al., "An overview on limitations of TiO_2-based particles for photocatalytic degradation of organic pollutants and the corresponding countermeasures," *Water Research*, vol. 79, pp. 128–146, 2015.

[14] A. Kutuzova and T. Dontsova, "Synthesis, characterization and properties of titanium dioxide obtained by hydrolytic method," *Proceedings of the 2017 IEEE 7 th International Conference on nanomaterials: Applications and Properties*, 2017, pp. 286–290, Zatoka, Ukraine, 2017.

[15] J. Chen, J. Shi, X. Wang, H. Cui, and M. Fu, "Recent progress in the preparation and application of semiconductor/graphene

composite photocatalysts," *Chinese Journal of Catalysis*, vol. 34, no. 4, pp. 621–640, 2013.

[16] A. Sviderskyi, S. Nahirniak, T. Yashchenko, T. Dontsova, and S. Kalinowski, "Properties of TiO_2 and SnO_2 in a state of different dispersion and morphology," *Proceedings of the 2018 IEEE 8th International Conference Nanomaterials: Application and Properties*, 2018, pp. 1–4, Zatoka, Ukraine, 2018.

[17] A. T. Kuvarega and B. B. Mamba, "TiO_2-based Photocatalysis: Toward Visible Light-Responsive Photocatalysts Through Doping and Fabrication of Carbon-Based Nanocomposites," *Critical Reviews in Solid State and Materials Sciences*, vol. 42, no. 4, pp. 295–346, 2016.

[18] H. C. Lee, H. S. Park, S. K. Cho et al., "Direct photoelectrochemical characterization of photocatalytic H, N doped T powder suspensions," *Chemical Reviews*, vol. 17, pp. 56–60, 2017.

[19] H. Luo, Z. Zeng, G. Zeng et al., "Recent progress on metal-organic frameworks based- and derived-photocatalysts for water splitting," *Chemical Engineering Journal*, vol. 383, p. 123196, 2020.

[20] J. Wen, X. Li, W. Liu, Y. Fang, J. Xie, and Y. Xu, "Photocatalysis fundamentals and surface modification of TiO_2 nanomaterials," *Chinese Journal of Catalysis*, vol. 36, no. 12, pp. 2049–2070, 2015.

[21] Y. Zhu, Z. Zhang, N. Lu, R. Hua, and B. Dong, "Prolonging charge-separation states by doping lanthanide-ions into {001}/{101} facets-coexposed TiO_2 nanosheets for enhancing photocatalytic H_2 evolution," *Chinese Journal of Catalysis*, vol. 40, no. 3, pp. 413–423, 2019.

[22] X. Li, J. Yu, M. Jaroniec, and X. Chen, "Cocatalysts for selective photoreduction of CO_2 into solar fuels," *Chemical Reviews*, vol. 119, no. 6, pp. 3962–4179, 2019.

[23] M. Huang, J. Yu, B. Li et al., "Intergrowth and coexistence effects of TiO_2–SnO_2 nanocomposite with excellent photocatalytic activity," *Journal of Alloys and Compounds*, vol. 629, pp. 55–61, 2015.

[24] A. Kutuzova, T. Dontsova, and W. Kwapinski, "TiO_2–SnO_2 nanocomposites: effect of acid–base and structural-adsorption properties on photocatalytic performance," *Journal of Inorganic and Organometallic Polymers and Materials*, vol. 30, no. 8, pp. 3060–3072, 2020.

[25] R. Bargougui, A. Pichavant, J.-F. Hochepied, M.-H. Berger, A. Gadri, and S. Ammar, "Synthesis and characterization of SnO_2, TiO_2 and $Ti_{0.5}Sn_{0.5}O_2$ nanoparticles as efficient materials for photocatalytic activity," *Optical Materials*, vol. 58, pp. 253–259, 2016.

[26] A. Kusior, J. Klich-Kafel, A. Trenczek-Zajac, K. Swierczek, M. Radecka, and K. Zakrzewska, "TiO_2–SnO_2 nanomaterials for gas sensing and photocatalysis," *Journal of the European Ceramic Society*, vol. 33, no. 12, pp. 2285–2290, 2013.

[27] D. Nithyadevi and R. T. Rajendrakumar, "Synthesis, characterization and photocatalytic properties of TiO_2–SnO_2 composite nanoparticles," *Advanced Materials Research*, vol. 678, pp. 373–377, 2013.

[28] M. Hirano and T. Kono, "Synthesis of Rutile-Type TiO_2-SnO_2 Solid Solution Nanoparticles by "Forced Co-Hydrolysis" under Hydrothermal Conditions," *IOP Conference Series: Materials Science and Engineering*, vol. 18, no. 6, 2011.

[29] T. Dontsova, I. Ivanenko, and I. Astrelin, "Synthesis and characterization of titanium (IV) oxide from various precursors," *Springer Proceedings in Physics*, vol. 167, pp. 275–293, 2015.

[30] M. A. Vargas and J. E. Rodríguez-Páez, "Amorphous TiO_2 nanoparticles: synthesis and antibacterial capacity," *Journal of Non-Crystalline Solids*, vol. 459, pp. 192–205, 2017.

[31] Q. Wang, X. Wei, J. Dai, J. Jiang, and X. Huo, "Influence of annealing process on ferromagnetism of undoped TiO_2 nanoparticles prepared by sol–gel method," *Materials Science in Semiconductor Processing*, vol. 21, pp. 111–115, 2014.

[32] A. S. Kutuzova and T. A. Dontsova, "Characterization and properties of TiO_2–SnO_2 nanocomposites, obtained by hydrolysis method," *Applied Nanoscience*, vol. 9, no. 5, pp. 873–880, 2019.

[33] T. Ivanova, A. Harizanova, T. Koutzarova, and B. Vertruyen, "Optical and structural characterization of TiO_2 films doped with silver nanoparticles obtained by sol–gel method," *Optical Materials*, vol. 36, no. 2, pp. 207–213, 2013.

[34] N. Liu, X. Chen, J. Zhang, and J. W. Schwank, "A review on TiO_2-based nanotubes synthesized via hydrothermal method: formation mechanism, structure modification, and photocatalytic applications," *Catalysis Today*, vol. 225, pp. 34–51, 2014.

[35] I. A. Kovalev, A. A. Petrov, O. A. Ibragimova et al., "New hierarchical titania-based structures for photocatalysis," *Mendeleev Communications*, vol. 28, no. 5, pp. 541-542, 2018.

[36] A. Kutuzova and T. Dontsova, "TiO_2-SnO_2 nanocomposites obtained by hydrothermal method," *International Conference Nanomaterials: Application & Properties (NAP)*, pp. , 20181–5, 2018.

[37] H. Rasoulnezhad, G. Kavei, K. Ahmadi, and M. R. Rahimipour, "Combined sonochemical/CVD method for preparation of nanostructured carbon-doped TiO_2 thin film," *Applied Surface Science*, vol. 408, pp. 1–10, 2017.

[38] R. Wittawat, R. Rittipun, M. Jarasfah, and B. Nattaporn, "Synthesis of ZnO/TiO_2 spherical particles for blue light screening by ultrasonic spray pyrolysis," *Materials Today Communications*, vol. 24, p. 101126, 2020.

[39] L. G. Bettini, M. V. Dozzi, F. D. Foglia et al., "Mixed-phase nanocrystalline TiO_2 photocatalysts produced by flame spray pyrolysis," *Applied Catalysis B: Environmental*, vol. 178, pp. 226–232, 2015.

[40] M. Scarisoreanu, C. Fleaca, I. Morjan et al., "High photoactive TiO_2/SnO_2 nanocomposites prepared by laser pyrolysis," *Applied Surface Science*, vol. 418, pp. 491–498, 2017.

[41] S. Bouhadoun, C. Guillard, F. Dapozze et al., "One step synthesis of N-doped and Au-loaded TiO_2 nanoparticles by laser pyrolysis: application in photocatalysis," *Applied Catalysis B: Environmental*, vol. 174-175, pp. 367–375, 2015.

[42] S. Anandan, N. Pugazhenthiran, T. Lana-Villarreal, G.-J. Lee, and J. J. Wu, "Catalytic degradation of a plasticizer, diethylhexyl phthalate, using N_x–TiO_{2-x} nanoparticles synthesized via co-precipitation," *Chemical Engineering Journal*, vol. 231, pp. 182–189, 2013.

[43] M. Zikriya, Y. F. Nadaf, P. V. Bharathy, and C. G. Renuka, "Luminescent characterization of rare earth Dy^{3+} ion doped TiO_2 prepared by simple chemical co-precipitation method," *Journal of Rare Earths*, vol. 37, no. 1, pp. 24–31, 2019.

[44] D. Hariharan, P. Thangamuniyandi, P. Selvakumar et al., "Green approach synthesis of Pd@TiO_2 nanoparticles: characterization, visible light active picric acid degradation and anticancer activity," *Process Biochemistry*, vol. 87, pp. 83–88, 2019.

[45] V. R. de Mendonça, W. Avansi Jr., R. Arenal, and C. Ribeiro, "A building blocks strategy for preparing photocatalytically active anatase TiO_2/rutile SnO_2 heterostructures by hydrothermal annealing," *Journal of Colloid and Interface Science*, vol. 505, pp. 454–459, 2017.

[46] Y. Wang, C. Ma, C. Wang et al., "Design of SnO_2@Air@TiO_2 hierarchical urchin-like double-hollow nanospheres for high

performance dye-sensitized solar cells," *Solar Energy*, vol. 189, pp. 412–420, 2019.

[47] T. A. Dontsova, E. I. Yanushevskaya, S. V. Nahirniak et al., "Directional control of the structural adsorption properties of clays by magnetite modification," *Journal of Nanomaterials*, vol. 2018, Article ID 6573016, 9 pages, 2018.

[48] A. Das, P. Dagar, S. Kumar, and A. K. Ganguli, "Effect of Au nanoparticle loading on the photo-electrochemical response of Au–P25–TiO_2 catalysts," *Journal of Solid State Chemistry*, vol. 281, p. 121051, 2020.

[49] S. Tsunekawa, J. Kang, K. Asami, Y. Kawazoe, and A. Kasuya, "Corrigendum to Size and time dependences of the valence states of Sn ions in amphoteric tin oxide nanoparticles," *Applied Surface Science*, vol. 206, no. 1–4, pp. 1–74, 2003.

[50] D. Barreca, S. Garon, E. Tondello, and P. Zanella, "SnO_2 nanocrystalline thin films by XPS," *Surface Science Spectra*, vol. 7, no. 2, pp. 81–85, 2000.

[51] M. Kwoka, L. Ottaviano, M. Passacantando, S. Santucci, G. Czempik, and J. Szuber, "XPS study of the surface chemistry of L-CVD SnO_2 thin films after oxidation," *Thin Solid Films*, vol. 490, no. 1, pp. 36–42, 2005.

[52] C. Jia, H. S. Chen, and P. Yang, "Construction of hollow waxberry-like rutile-/anatase-TiO_2/SnO_2 towards enhanced photocatalysis," *Journal of Industrial and Engineering Chemistry*, vol. 58, pp. 278–289, 2018.

[53] D. Toloman, O. Pana, M. Stefan et al., "Photocatalytic activity of SnO_2-TiO_2 composite nanoparticles modified with PVP," *Journal of Colloid and Interface Science*, vol. 542, pp. 296–307, 2019.

[54] F. Wu, X. Li, W. Liu, and S. Zhang, "Highly enhanced photocatalytic degradation of methylene blue over the indirect all-solid-state Z-scheme g-C_3N_4-RGO-TiO_2 nanoheterojunctions," *Applied Surface Science*, vol. 405, pp. 60–70, 2017.

[55] M. Thommes, K. Kaneko, A. V. Neimark et al., "Physisorption of gases, with special reference to the evaluation of surface area and pore size distribution (IUPAC Technical Report)," *Pure and Applied Chemistry*, vol. 87, no. 9–10, pp. 1051–1069, 2015.

[56] O. Makarchuk, T. Dontsova, A. Perekos, A. Skoblik, and Y. Svystunov, "Magnetic mineral nanocomposite sorbents for wastewater treatment," *Journal of Nanomaterials*, vol. 2017, Article ID 8579598, 7 pages, 2017.

[57] R. Mimouni, B. Askri, T. Larbi, M. Amlouk, and A. Meftah, "Photocatalytic degradation and photo-generated hydrophilicity of methylene blue over ZnO/$ZnCr_2O_4$ nanocomposite under stimulated UV light irradiation," *Inorganic Chemistry Communications*, vol. 115, p. 107889, 2020.

[58] J. Shen, R. Wang, Q. Liu, X. Yang, H. Tang, and J. Yang, "Accelerating photocatalytic hydrogen evolution and pollutant degradation by coupling organic co-catalysts with TiO_2," *Chinese Journal of Catalysis*, vol. 40, no. 3, pp. 380–389, 2019.

[59] X. Li, J. Xiong, Y. Xu, Z. Feng, and J. Huang, "Defect-assisted surface modification enhances the visible light photocatalytic performance of g-C_3N_4@C-TiO_2 direct Z-scheme heterojunctions," *Chinese Journal of Catalysis*, vol. 40, no. 3, pp. 424–433, 2019.

[60] L. Hu, J. Yan, C. Wang, B. Chai, and J. Li, "Direct electrospinning method for the construction of Z-scheme TiO_2/g-C_3N_4/RGO ternary heterojunction photocatalysts with remarkably ameliorated photocatalytic performance," *Chinese Journal of Catalysis*, vol. 40, no. 3, pp. 458–469, 2019.